

P145 DEVELOPMENT OF A SHORT-RANGE PROBABILISTIC PRECIPITATION FORECAST ALGORITHM BASED ON RADAR AND NUMERICAL PREDICTION MODEL INPUT

David Kitzmiller*, Wanru Wu, Shaorong Wu, and Dennis Miller
Office of Hydrologic Development, NOAA National Weather Service, Silver Spring, MD

1. INTRODUCTION

Hydrologic Analysis Support forecasters at River Forecast Centers presently make use of centrally-produced precipitation guidance, and recent remote-sensor data from radar and satellite, to produce short-range quantitative precipitation forecasts (QPFs) for river forecasting. At present, the methods for blending these data are almost completely subjective. This task is especially challenging in situations where large, evolving mesoscale systems impact entire river basins.

Automated precipitation forecast systems that combine information from numerical weather prediction model forecasts and remote sensors have been implemented in a number of settings. (Sokol and Pešice 2009; Li and Lai 2004; Pierce et al. 2004). Direct application of radar nowcasting tools to hydrologic prediction has recently been tested in a number of applications (see for example Ganguly and Bras 2003; Vivoni et al. 2007).

An effort to develop and test an advective-statistical method for short-range QPFs has been undertaken by the NOAA National Weather Service (NWS) Office of Hydrologic Development. Here, we report on a new, regression-based technique that combines information from a numerical weather model and an advective-statistical nowcaster.

This technique ingests radar and satellite precipitation rate estimates and forecasts of the Rapid Update Cycle 2 (RUC2, hereafter referred to as RUC; Benjamin et al. 2004) operational numerical prediction model. It includes advective components for the radar and satellite fields, and directly inputs precipitation and humidity

forecasts from the RUC. Of particular interest is the fact that the RUC itself is initialized with three-dimensional radar reflectivity (Weygandt et al. 2007); hence we wished to determine if there is additional value to be gained from further radar input, through the extrapolation model.

Here, we describe development methodology, results for a recent heavy precipitation event, and the skill level of the QPFs relative to currently-available operational products, namely RUC forecasts and human-produced forecasts of the NCEP Hydrometeorological Prediction Center.

2. COMPONENTS OF THE FORECAST SYSTEM

Our developmental QPF model (hereafter denoted RS-REG for **R**emote-**S**ensor **R**EGression) incorporates both remote-sensor-driven extrapolative forecasts and physical/dynamical numerical weather prediction model forecasts. A statistical regression procedure is used to produce an optimally-weighted combination of the inputs relative to the desired predictands, which are probability of precipitation ≥ 0.25 , 2.5, 12.5, 25, 50, and 75mm in a 6-h period. Hereafter these forecasts are referred to as P(0.25mm), P(2.5mm), and so on. A QPF amount forecast is derived by comparing the probability forecasts P(2.5mm), P(12.5mm), P(25mm), and P(50mm) to a set of threshold values. The forecast fields are defined on a grid mesh of approximately 4 km, and are valid for the periods 0000-0600, 0600-1200, 1200-1800, and 1800-0000 UTC.

2.1 Remote sensor, numerical prediction, and developmental inputs

Radar precipitation rate input is taken from the prototype National Mosaic and Multisensor Quantitative Precipitation Estimation System (NMQ, Zhang et al., 2011). Satellite precipitation rate input is

**Contact: David Kitzmiller, W/OHD-12,
1325 East West Highway, Silver Spring
Maryland, <david.kitzmiller@noaa.gov>**

from the operational Hydroestimator algorithm (Scofield and Kuligowski 2003). Lightning strike input is taken from the National Lightning Detection Network (Orville et al 2008).

To account for the possibility that the extrapolation and RUC forecasts might have time-dependent influences on the final 6 h forecasted precipitation amount, we input as predictors separate forecasts for the first and second halves of the valid period, as well as the 6-h total amount forecast.

The current precipitation predictor input data can be summarized as follows:

- Initial-time radar and Hydroestimator precipitation rates, and lightning strike rates;
- 0-3h, 3-6h, and 0-6h radar- and satellite-derived rainfall amount, and lightning strike count, estimated by extrapolation;

- 0-3h, 3-6h, and 0-6h RUC rainfall amount;

- RUC stability indices, relative humidity, and precipitable water at the start of the valid period;

The remote sensor input is the latest that is operationally available up to about 10 minutes prior to the start of the valid period, to allow for processing time in order to complete the forecasts by the start of the valid period. The radar input is based on data at 15 minutes prior to initial time, the satellite input from infrared imagery at 45 minutes prior to initial time, and lightning input from the 15-minute period starting 40 minutes prior to initial time. The RUC inputs are from the model run initiated one hour prior to the valid period.

The development stage (but not real-time forecasting) requires ground validation precipitation estimates. These were taken from the Stage IV gauge/radar analysis, produced at NWS River Forecast Centers and spatially composited at NCEP (Lin and Mitchell, 2005). The StageIV data are defined on the same 4-km grid mesh that defines the QPF model output fields.

2.2 Extrapolation-Advection Model in RS-REG

While extrapolation of radar echoes and cloud patterns is generally effective out to a few hours, estimation of future

precipitation motion beyond about three hours is problematic because the patterns are generally forecasted to move into clear areas where no precipitation existed at the initial time. For prediction of echo motion as far ahead as six hours, we have applied a combination of extrapolation (future motion estimated from the previous motion of the echo pattern) and advection (future motion estimated from the lower tropospheric wind field). The initial-time echo motion field features extrapolation vectors based on lag-correlation pattern matching between recent radar image pairs, using a method now applied operationally in the High-Resolution Precipitation Nowcaster (Guan et al., 2005). These vectors are spatially blended with the NWP mid-tropospheric field in clear areas. At 1-h intervals, the motion field is updated such that the vectors tend toward the RUC-forecasted wind field. This updating is done by successively averaging the initial-time motion field with the RUC wind forecasts, placing increasing weight on the RUC fields until at 5 hours, the storm motion is entirely from the wind fields. Experimentation showed that this method produces realistic echo pattern evolution, and the resulting extrapolation QPFs are at least as skillful as those of the RUC.

3. STATISTICAL PREDICTION MODEL DEVELOPMENT

3.1 Data sample for development

A developmental data pool was formed by drawing predictor and predictand values from points at 0.25° latitude-longitude intervals, during the period April 2009 – March 2011, over the conterminous United States. Figure 1 shows this selection grid. Data for one case in the development sample consists of all predictor values and predictand (observed precipitation) values at one point during one forecast period on one day. After all data were collected, forward-selection screening regression was used to select predictor combinations for the various predictands.

The data sample included only cases with at least one predictor among the radar, satellite, and RUC variables indicating precipitation ≥ 0.25 mm. In practice this sample captures all but a very few significant precipitation events. Due to the

need for forecasts outside the radar network, or in areas of the CONUS poorly served by radar at present, backup equations using only RUC and Hydroestimator predictors, but not radar, were also derived, and applied as explained below.

Examining some of the predictor/predictand relationships for the 50- and 75-mm threshold values indicated the need to account for nonlinear predictor/predictand joint distributions. Accordingly, we prepared two-predictor contingency tables to determine the nature of the relationship. The relationships were generally well-described by a biquadratic equation, such as an expression for P(50mm) based on radar and RUC 0-6h precipitation forecasts:

$$\text{BIQUAD-50mm} = 0.217 + 0.023 \text{ RUCP} - 0.024 \text{ RADP} - 0.0012 \text{ RUCP}^2 + 0.0013 \text{ RADP}^2 + 0.0041 \text{ RUC RADP}$$

where RADP is the radar forecast (mm), RUCP is the RUC forecast (mm), and BIQUAD-50mm is in percent. These predictor relationships were derived from data for all forecast periods based on data from the entire CONUS, then offered to the screening regression as new predictors. The linear regression procedure and geographic localization procedures explained below adjust the probabilities higher or lower to agree with local climatology.

A probability equation typical of many in the central United States is that for P(2.5mm) at latitude 36°N, -90 °E during the 1800-0000 UTC valid period:

$$P(2.5\text{mm}) = -0.0197 + 0.0434 [\text{RAD-RUC BIQUAD}] + 0.0188 [\text{SAT-RUC BIQUAD}]$$

where P is a fraction (0-1), RAD-RUC-BIQUAD is a biquadratic expression involving the 0-6h radar precipitation forecast and RUC 0-6h precipitation forecasts, defined in mm; and SAT-RUC BIQUAD is a biquadratic expression relating the Hydroestimator and RUC 0-6h precipitation amount forecasts to the probability of 25-mm precipitation, defined in per cent Note that expressions for precipitation amount and for probability were

both commonly selected as probability predictors.

3.2 Geographic localization of forecast equations

Because of the climatic diversity of precipitation across the conterminous United States, we stratified the development subsamples by geography, the valid time period, and warm and cool seasons, namely April-September and October-March respectively.

Examination of the precipitation-based predictors and StageIV estimates showed that in broad-scale terms, the predictors clearly reflect geographic variations in precipitation, though with some characteristic biases. In some cases the biases can change appreciably in small spatial intervals, indicating a need for geographic stratification. This stratification must usually be carried out on regions of at least 10,000 km², in order to collect enough of the high-precipitation events to obtain reliable regression relationships (Charba and Samplatsky 2011a).

While it is possible to define fixed, irregularly shaped regions that reflect major topographic and climatic regions, the definition process has some subjectivity, and subsequently there might be a need for smoothing of the forecast fields near region boundaries (Charba and Samplatsky 2011b). Our approach was designed to bypass this regionalization procedure by drawing subsamples of cases from within floating, overlapping latitude-longitude windows of 3x3°, 5x5°, and 7x7° dimensions, centered at 1° intervals. The rectangular boxes in Fig. 1 indicate the approximate size of these areas. At least 1500 individual precipitation cases were required to attempt to identify a regression relationship; often 20,000 cases were available within a 3x3° box. However, for dry regions and the lower-frequency high precipitation events, it was necessary to specify a sample from the 5x5° or 7x7° box to obtain a sufficient sample and a realistic regression equation. The equation from the smallest possible box is used in real-time prediction.

This procedure yielded equations at 750 to 900 latitude-longitude points. It was not possible to obtain regression

relationships for some of the higher amount thresholds in the driest parts of the western United States, even from the largest sampling box. The central latitude-longitude point is considered the nominal location of any given equation. The regression coefficients applied at any point of the 4-km forecast grid are those from the closest location. This convention supplied equation coefficients at all forecast grid boxes. Finally, a smoothing procedure was applied to all equation coefficient values at all points, resulting in a continuous spatial transition in the coefficients.

3.3 Forecast equations in and near radar coverage gaps

Because of known coverage gaps in the WSR 88D network (Maddox et al. 2002), it is necessary to treat the contingency of forecasts where the radar-based component is generally zero. In previous work (Wu and Kitzmiller 2011), a form of radar coverage map was derived through estimation of the long-term correlation between NMQ daily precipitation and forecasts of the North American Mesoscale model. At any one geographic point, this correlation value serves as a measure of radar quality. Based on comparisons with known geographic coverage gaps, wherever this correlation was < 0.5 , it was assumed the radar coverage was suspect for forecasting purposes. However, it is still possible for radar precipitation from nearby areas of good coverage to be advected into the area of poor coverage. Therefore, the forecast values from the current radar-based and satellite-based estimates are compared, and that giving the higher probability is applied at that geographic location.

3.4 Commonly-selected predictors for probability equations

Results from the screening regression procedure showed that the most useful predictors for all amount thresholds included the RUC and 0-6h radar precipitation forecasts, and the nonlinear combination predictors derived from them; 1000-500hPa mean relative humidity from RUC forecasts; and the 3-6h RUC precipitation forecasts. Though they were offered for screening, the initial-time radar and satellite precipitation

rates, and lightning-based predictors, were rarely selected, since they possess limited information about the remainder of the 6-h forecast period. Over about 5% of the total area, mainly in the western portions, the satellite-based predictors were selected rather than radar-based, likely a reflection of radar coverage limitations.

3.5 Deterministic amount forecasts based on probability forecasts

While probability forecasts are informative, hydrologic applications generally require a precipitation amount forecast. To derive this forecast while employing information from the probability forecasts, we employed a method similar to that described by Charba and Samplatsky (2011a), who applied a set of threshold criteria to the probability forecasts at any one point to derive an amount forecast for that point.

Our approach is based on determining probability forecast values that occur at the same relative frequency as certain observed precipitation amount thresholds, within the 2009-2011 development data sample. For example, P(2.5mm) probability forecasts ≥ 0.14 occur as often as observed precipitation ≥ 0.25 mm; therefore this probability value is treated as a threshold for an amount forecast of 0.25mm. At any point where this threshold is exceeded, the P(2.5mm) is compared to successively higher thresholds to determine higher precipitation amount forecasts up to 15mm.

If the P(2.5mm) exceeds 0.9, the P(12.5mm) forecast is compared to thresholds to define amount forecasts from 15 to 30mm. If the P(12.5mm) value exceeds 0.6, the 25-mm probability forecast is tested to estimate amounts up to 50 mm, and 50-mm probabilities apply to amounts above 50mm.

This approach yielded a distribution of forecast amounts closely approximating the observed distribution, within the development sample, and it was anticipated that the relationships would hold for independent data.

4. EXAMPLE OF INPUT AND RESULTING FORECAST FIELDS

An illustration of the forecast procedure including input from the T.S. "Lee" event of September 2011 is shown in Fig. 2. Both NMQ radar and Hydroestimator satellite algorithms indicated extensive heavy rainfall over the eastern United States around 1130 UTC on 5 September (Fig. 2a,b). The extrapolation/advection procedure outlined above resulted in the forecast precipitation patterns for the 1200-1800 UTC period shown in Fig. 2c,d; these are similar to the RUC forecast valid during the same period (Fig. 2e). Some amounts in excess of 75mm (3 inches) were indicated by these input forecasts.

The regression equations applied to this radar, satellite, and RUC input resulted in probability forecasts P(2.5mm), P(25mm), and P(50mm) as appear in Fig. 2f-h. As would be expected, the highest probabilities are in the area from eastern Alabama through northern Mississippi, into Tennessee and Kentucky. Some P(25mm) values were in excess of 60%, and P(75mm) values in excess of 15%, which are exceptionally high values. High probabilities were also indicated in the path of intense convection over smaller areas extending into the northeastern United States.

Through the threshold comparison procedure described in Section 3, the probability forecasts define a QPF amount forecast, as illustrated schematically in Fig. 3a-e. The amount forecast (Fig. 3e) featured values in excess of 75mm over Alabama, and values above 25mm over a large surrounding area, as well as farther northeast. The forecast grid from HPC (Fig. 3f) features less spatial detail, because of its issuance at a larger grid mesh length of 32 km, but this forecast also indicates a maximum over 75mm.

StageIV gauge-radar estimates for the valid period (Fig. 3g) showed amounts in excess of 75mm and some in excess of 100mm over Alabama and Mississippi; rainfall in excess of 50 mm was also estimated over Tennessee and eastern Kentucky, the Florida Panhandle, and extreme northeastern Georgia. Some values above 25mm were observed as far north as New York, Vermont, and Quebec. The overall pattern was clearly reflected in

the forecast probability and amount fields, though some features such as the areas of heaviest rainfall over Pennsylvania and New York were not captured. These might have been due to subsequent development of embedded convection.

5. VERIFICATION RESULTS AND DISCUSSION

Following final development of the forecast probability equations with data from the period April 2009 through March 2011, we prepared a limited verification test with cases from April-June 2011. The warm-season probability forecast equations were applied to these data, and then evaluated in several ways. We also compared the scores to those for the RUC model, and for forecasts of the NCEP Hydrometeorological Prediction Center (HPC), which are prepared for the same valid periods and issued in gridded form (Olson et al. 1995).

This verification was carried out within a sample similar to that for the development dataset, that is, only including cases with RUC, radar or satellite precipitation forecasting ≥ 0.25 mm precipitation. This sample features cases with at least some minimal chance for precipitation recognizable in advance. We found that the regression, HPC, and RUC forecasts rarely differed greatly in the size and shape of forecasted precipitation regions, therefore this appears to be a reasonable standard for evaluation. For this evaluation, a subset of ~200,000 randomly-selected forecasts from each of the four valid periods was tested. To this point, no geographic breakdown of the verification statistics has been attempted.

A primary concern is that the forecasts are reliable, that is, the mean forecast closely approximates the mean observation. As shown in Fig. 4, the mean RS-REG QPF amount forecast is very close to that of the observed, while the RUC forecasts have a high bias during the daytime periods, and HPC forecasts have a slight high bias in general.

Examination of probability forecasts for the 1800-0000 UTC valid period (Fig.5) showed good reliability for the forecasts of 12.5- and 25-mm events, while the occurrence of 0.25 and 2.5 mm was under-forecasted, by about 20% and 15%

respectively. The rare 50-mm and 75-mm events (not shown) were over-forecasted. Similar results were found for the other three valid periods.

The accuracy of the amount forecasts was evaluated in terms of the root-mean-square-error (RMS). Here, we found that the RS-REG produced poorer results than either the HPC forecasts or RUC forecasts (Fig. 6a). This is despite the fact that the RS-REG forecasts clearly had a higher rank correlation with observations than did the RUC in both the development and the verification samples (verification sample results shown in Fig. 6b). Further examination revealed that this could be due to an excessive number of large RS-REG forecasts > 50mm within the verification sample. Though the amount forecasts were well-calibrated within the development sample of data from 2009-2011, they did not properly match the high end of the observed distribution in the 2011 sample. This indicates a need for redevelopment of the equations with more data.

We did, however, determine that for the higher precipitation thresholds > 25mm, the information content of the RS-REG probability forecasts was clearly higher than that of the RUC component, and generally competitive with that of the HPC forecasts. To illustrate this finding, we converted the RS-REG probability forecasts, and the HPC and RUC amount forecasts, to yes/no forecasts corresponding to thresholds of 25, 50, and 75mm. These were then scored in terms of probability of detection (POD) and critical success index (CSI). These are defined:

$$\text{POD} = X / (X+Y); \text{CSI} = X / (X + Y + Z)$$

where X is the count of detected precipitation events (“hits”), Y the count of missed precipitation events, and Z is the count of cases where the event was forecasted but not observed (false alarms)

For all three sets of forecasts, a range of yes/no conversion thresholds was tested; the HPC and RUC forecasts were only rarely above 50mm and relying on the actual amount forecasts resulted in detection of < 0.05 of observed events. The goal was to find the conversion threshold yielding the maximum CSI, subject to $\text{POD} \geq 0.25$. The value of the HPC or RUC

forecasts was generally maximized by selecting a threshold lower than the stated value, for example, all forecasts $\geq 30\text{mm}$ would be converted to a 50mm “yes” forecast. For the RS-REG forecasts, a range of conversion probability thresholds was tested.

When the forecasts and observations were examined in terms of maximum CSI, we found that the HPC forecasts generally yielded the highest values for the 25-mm threshold for all four forecast periods (Fig. 7a), while for the 50- and 75-mm thresholds the RS-REG forecasts were close to or higher than the HPC values (Fig. 7b,c). The exception was for the 1800-0000 UTC period, when the HPC values were much higher than either RS-REG or RUC. Given that the CSI was generally correlated among the three forecasts, it is possible that this last result is due to chance and the rarity of the 50- and 75-mm events. However we note that the RS-REG scores were consistently higher than those for the RUC in all four valid periods.

Since the purpose of this development effort was to provide an adjunct guidance product to that currently available, we investigated some possibilities for considering the HPC and RS-REG forecasts together. Examination of cases with a clear potential for high rainfall revealed that, if any one among the RUC, HPC, or RS-REG forecasts indicated a high amount > 25mm, then the most additional information could be obtained by reference to one of the other forecast systems. For example, within the set of ~6,000 cases in which the HPC forecast was $\geq 25\text{mm}$, the RUC and RS-REG forecasts were more highly correlated with observed 25-mm events than was the HPC forecast itself. As shown in Table 1, there was clearly independent information in the RS-REG forecasts, such that if the RS-REG QPF was also $\geq 25\text{mm}$, the probability of an observed event was appreciably higher than if the RS-REG forecast was < 15mm (0.43 vs. 0.26).

6. CONCLUSIONS

A prototype system for merging information from radar, satellite, and numerical prediction model QPF was

developed. To create the prototype, a set of regression relationships were derived between an observed predictand, namely StageIV gauge-radar gridded precipitation analyses, and predictor variables derived from extrapolative/advective forecasts of precipitation amount based on radar and satellite information, and numerical forecasts of the RUC model. Following development with a two-year set of training data from 2009-2011, the RS-REG system was tested on new data from 2011. The results thus far confirm that information from extrapolation of radar and satellite remote sensor estimates of precipitation rate, and from the operational numerical RUC model, are complementary. We also saw evidence of the complementary nature of the automated RS-REG system and operational products produced by human forecasters at HPC. It should be noted that the very small verification area for each datum, 4x4 km or 16 km², represents a severe forecasting challenge, and absolute accuracy is likely higher over larger spatial domains.

At present, we operate the RS-REG system in real time within the Office of Hydrologic Development. Future operational deployment depends on positive evaluations by end users, particularly HPC and River Forecast Center staff. We are investigating possibilities for limited real-time dissemination of the prototype forecast products.

ACKNOWLEDGMENTS

Development of the RS-REG system is supported by the NOAA NWS Advance Hydrologic Prediction System (AHPS) initiative. We gratefully acknowledge comments and guidance received from staff of the Arkansas-Red River Basin River Forecast Center. Archived forecasts from HPC were kindly supplied by the NWS National Precipitation Verification Unit. NMQ radar grids were supplied by the NOAA National Severe Storms Laboratory. Hydroestimator satellite precipitation grids were supplied by NOAA NESDIS. Valuable insights on the development process were supplied by Zbyněk Sokol of the Institute of Atmospheric Physics, Czech Republic Academy of Sciences

REFERENCES

- Benjamin S. G., and coauthors, 2004: An hourly assimilation/forecast cycle: The RUC. *Mon. Wea. Rev.*, **132**, 495–518.
- Charba, J., and F. Samplatsky, 2011a: High-Resolution GFS-Based MOS quantitative precipitation forecasts on a 4-km grid. *Mon. Wea. Rev.*, **139**, 39–68.
- _____, and _____, 2011b: Regionalization in fine-grid GFS MOS 6-h quantitative precipitation forecasts. *Mon. Wea. Rev.*, **139**, 24–38.
- Ganguly, A., and R. Bras, 2003: Distributed quantitative precipitation forecasting using information from radar and numerical weather prediction models. *J. Hydrometeor.*, **4**, 1168–1180.
- Guan, S., F. Ding, R. Fulton, and D. Kitzmiller, 2005: Preliminary results for the 0-1 hour multisensor precipitation nowcaster. *Preprints 32nd Conference on Radar Meteorology*, Amer. Meteor. Soc., 6R.4.
- Li, P., and E. Lai, 2004: Short-range Quantitative Precipitation Forecasting in Hong Kong. *J. Hydrol.*, **288**, 189-209.
- Lin, Y. and Mitchell, K. (2005). The NCEP Stage II/IV hourly precipitation analyses: Development and applications. *Preprints, 19th Hydrol. Conf.*, Amer. Meteor. Soc., Boston, MA, 1.2.
- Maddox, R., J. Zhang, J. Gourley, and K. Howard, 2002: Weather radar coverage over the Contiguous United States. *Wea. Forecasting*, **17**, 927–934.
- Olson, D. A., N. W. Junker, and B. Korty, 1995: Evaluation of 33 years of quantitative precipitation forecasting. *Wea. Forecasting*, **10**, 498–511.
- Orville, R.E., 2008: Development of the National Lightning Detection Network. *Bull. Amer. Meteor. Soc.*, **89**, 180–190.
- Pierce, C. E., and Coauthors, 2004: The nowcasting of precipitation during Sydney 2000: An appraisal of the QPF algorithms. *Wea. Forecasting*, **19**, 7–21.
- Scofield, R. A., and R. J. Kuligowski, 2003: Status and outlook of operational satellite precipitation algorithms for extreme-

precipitation events. *Wea. Fcst.*, **18**, 1037-1051.

Sokol, Z., P. Pešice, 2009: Comparing nowcastings of three severe convective events by statistical and NWP models. *Atmospheric Research*, **93**, 397-407.

Vivoni, E., D. Entekhabi, and R. Hoffman, 2007: Error propagation of radar rainfall nowcasting fields through a fully distributed flood forecasting model. *Journal of Applied Meteorology and Climatology*, **46**: 932-940.

Weygandt, S., S. Benjamin, and J. Brown, 2007: Radar reflectivity-based initialization of precipitation systems using a diabatic digital filter. *Preprints, 33rd International*

Radar Conference, Amer. Meteor. Soc., Cairns, Australia, 4A.6.

Wu, W., and D. Kitzmiller 2009: Evaluation of radar precipitation estimates from NMQ and WSR-88D Digital Precipitation Array products: Preliminary results. *Preprints 34th Conference on Radar Meteorology*, Williamsburg, Amer. Meteor. Soc., P14.4.

Zhang, J., and Coauthors, 2011: National Mosaic and Multi-sensor QPE (NMQ) System - Description, results and future plans. Accepted for publication in *Bull. Amer. Soc.*

—

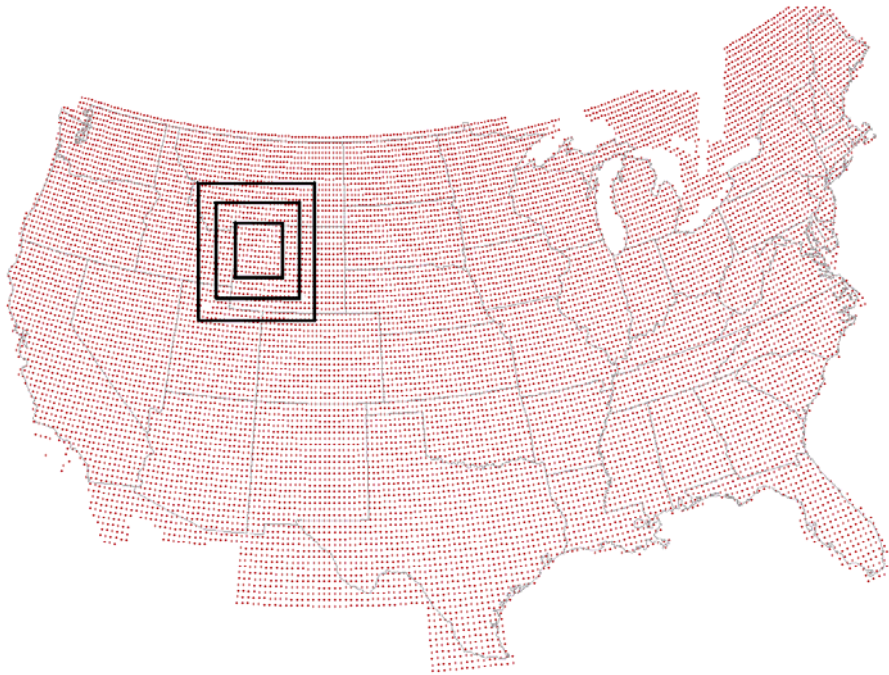
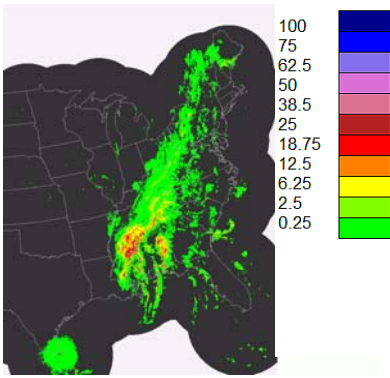


Figure 1. Distribution of data-sampling points applied in the process of developing regression equations; points fall at 0.25° intervals. Concentric boxes at upper left indicate the approximate size of the $3 \times 3^\circ$, $5 \times 5^\circ$, and $7 \times 7^\circ$ sampling boxes used in collecting samples for regression.

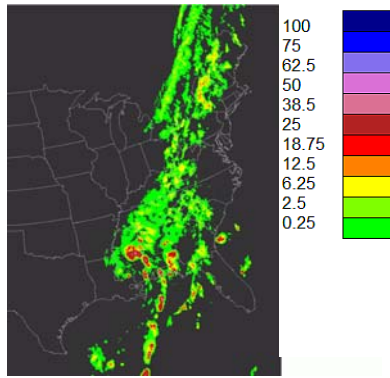
Initial radar precip rate

a



Initial satellite precip rate

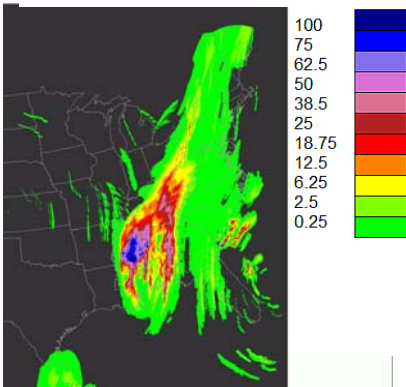
b



T.S. "Lee"
1200-1800 UTC
5 Sep 2011

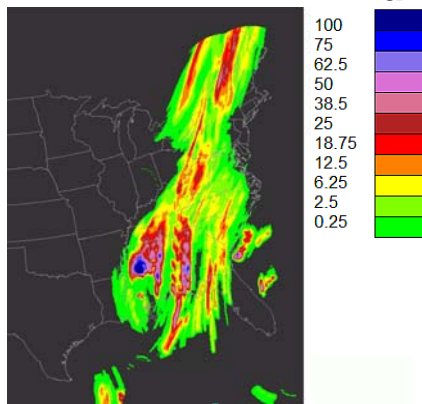
6-hQPF by extrapolation

c



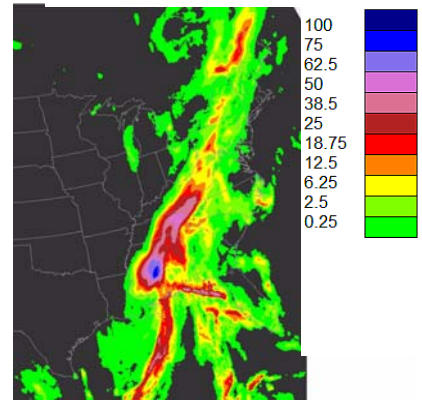
6-hQPF by extrapolation

d



6-h RUC Forecast

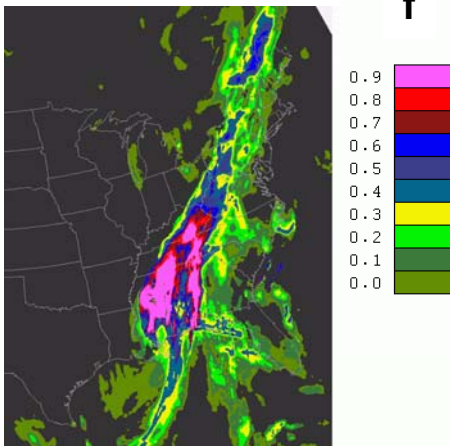
e



Probability equations relate extrapolation and RUC QPFs to precipitation probabilities

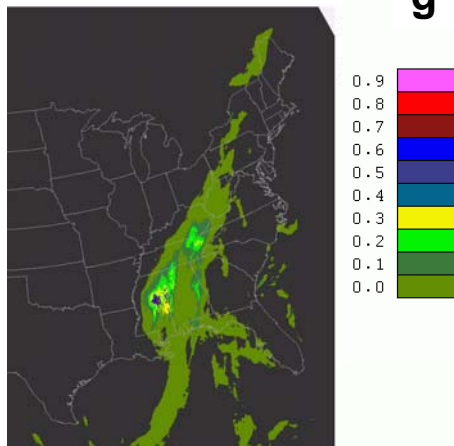
Probability >2.5mm

f



Probability >25mm

g



Probability >50mm

h

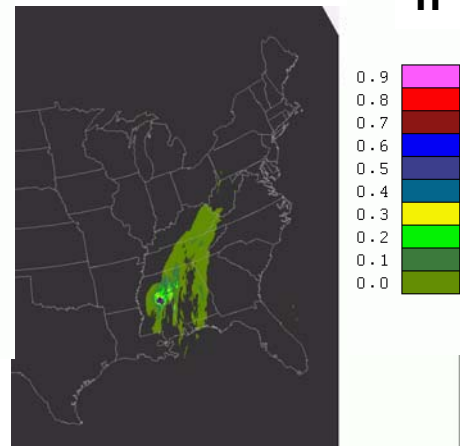


Figure 2. Input and RS-REG forecasts valid 1200-1800 UTC, 5 September 2011. Radar (a) and satellite (b) input are extrapolated to produce 6-h precipitation forecasts (c,d) which are statistically merged with the RUC numerical forecast (e). Probability forecasts (f-h) are derived from the extrapolation and RUC forecasts. Amounts are in mm, probabilities range 0-1; see color scales.

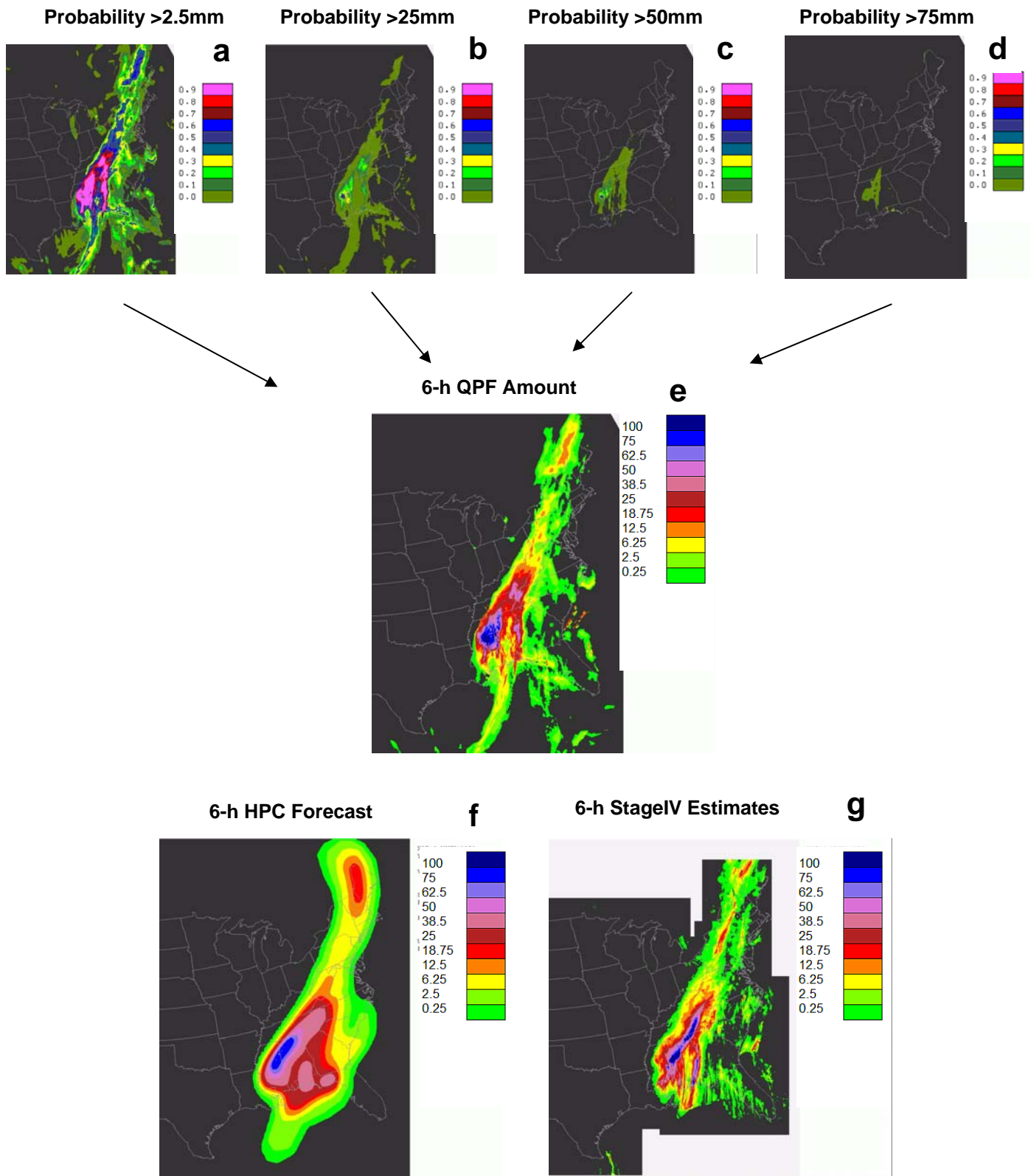


Figure 3. RS-REG forecasts valid 1200-1800 UTC, 5 September 2011, corresponding HPC forecast, and StageIV gauge-radar verification. Probability of exceeding thresholds of 2.5, 25, 50, and 75mm (a-d), and QPF amount (mm) (e). HPC forecast (f) has pattern similar to RS-REG. Some amounts in excess of 100mm were observed (g). Amounts and rates are in mm; probabilities 0-1 (see color scales).

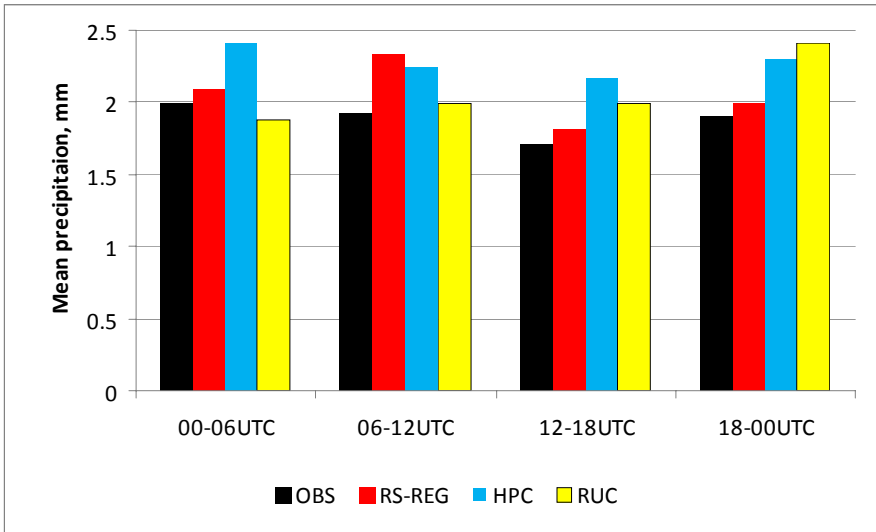


Figure 4. Mean observed and forecasted precipitation amounts. Values are for the period April-June 2011.

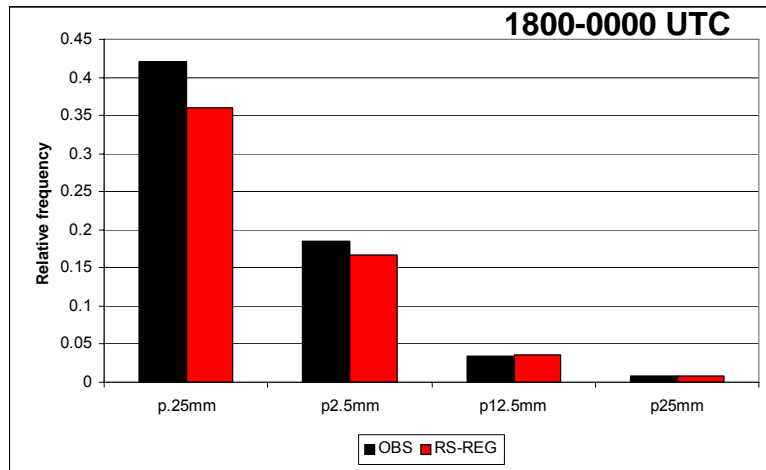


Figure 5. Relative frequency of observed precipitation events (black bars) and mean RS-REG probability forecasts (red bars) for valid periods (a) 0000-0600 and (b) 1800-0000 UTC.

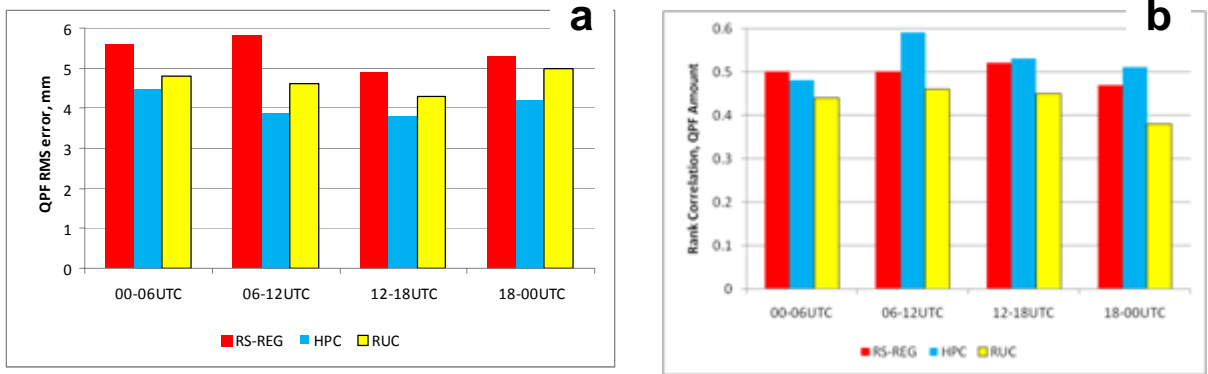


Figure 6. Root-mean squared error (a) and rank correlation (b) for precipitation amount forecasts; statistics are relative to StageIV verification, April-June 2011.

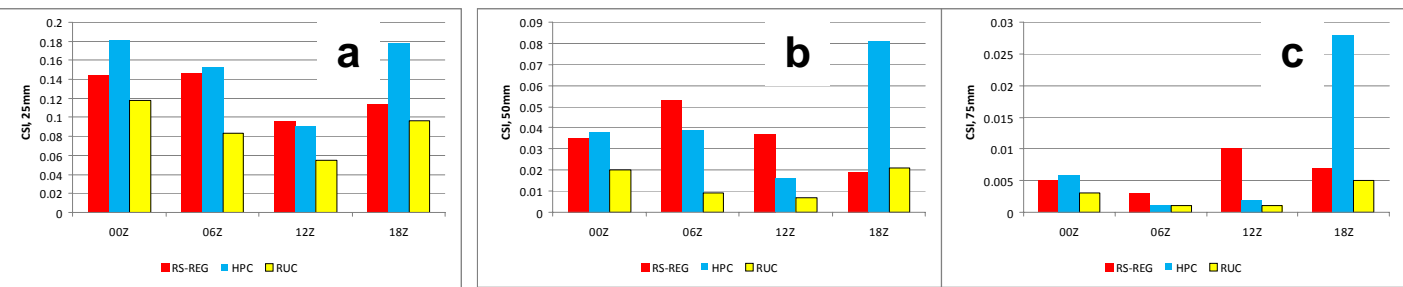


Figure 7. Maximum Critical Success Index (CSI) for RS-REG, HPC, and RUC forecasts, for (a) 25-mm events, (b) 50-mm events, and (c) 75-mm events. Maximum CSI value is subject to detection of at least 0.25 of the observed events.

Table 1. Fraction of cases with observed precipitation ≥ 25 mm, for different ranges of RS-REG QPF, given that HPC forecast was ≥ 25 mm. Within this sample, there is a clear relationship between the RS-REG QPF and event relative frequency, implying information independent of the HPC forecast.

Relative frequency of observed precipitation ≥ 25 mm	0.26	0.35	0.43
Precipitation amount forecasted by RS-REG	0-15mm	15-25mm	>25mm